IET Radar Sonar and Navigation, Volume 12, 2018, Issue 11, pp. 1320-1329
DOI: 10.1049/iet-rsn.2018.5029

IET Research Journals

Research Article

IET Journals
The Institution of Engineering and Technology

Multibeam radar based on linear frequency modulated waveform diversity

ISSN 1751-8644
doi: 0000000000
www.ietdl.org

Leon Kocjancic[1*], *Alessio Balleri*[1], *Thomas Merlet*[2]

[1] *Centre for Electronic Warfare, Information and Cyber, Cranfield University, Defence Academy of the UK, Shrivenham, SN6 8LA, United Kingdom*
[2] *Thales Optronique SAS, 2 Avenue Gay Lussac, Elancourt, 78995, France*
* *E-mail: leon.kocjancic@cranfield.ac.uk*

Abstract: Multibeam radar (MBR) systems based on waveform diversity require a set of orthogonal waveforms in order to generate multiple channels in transmission and extract them efficiently at the receiver with digital signal processing. Linear frequency modulated (LFM) signals are extensively used in radar systems due to their pulse compression properties, Doppler tolerance and ease of generation. In this paper, we investigate the level of isolation between MBR channels based on LFM chirps with rectangular and Gaussian amplitude envelopes. The orthogonal properties and the mathematical expressions of the isolation are derived as a function of the chirp design diversity, and specifically for diverse frequency slopes and frequency offsets. The analytical expressions are validated with a set of simulations as well as with experiments at C-band using a rotating target.

1 Introduction

Multiple input multiple output (MIMO) radars have attracted significant research interest in the last decade. Taxonomically, MIMO radar systems can be divided into several groups [1]. Monostatic and quasi-monostatic MIMO radars deploy co-located, or nearly co-located, antennas so that all nodes experience the same target radar cross section (RCS) [2, 3]. Statistical MIMO radars deploy widely-separated antennas and each radiating element sees a different target RCS due to the different aspect angle [4]. Finally, MIMO radar systems can also be synthesised using a network of non-cooperative radar systems.

A requirement common to all types of MIMO radars is high level isolation between channels. This can be achieved with well established techniques that provide almost perfect signal isolation, such as time division multiplexing (TDM) and frequency division multiplexing (FDM) [5–7]. However, the issue with these is they are often not feasible in practice due to hardware and operational limitations. For example, when a MIMO system is operated coherently, the target or background response varies with time and frequency and this inhibits the performance of TDM and FDM techniques. Another approach to achieve channel isolation is based on code division multiplexing (CDM) or, more generally, on waveform diversity (WD) techniques. These are based on orthogonal codes, or signals, that interleave in the time and frequency domain. For these systems, the design of the waveforms employed and their orthogonal properties are the key to provide the desired MIMO radar performance.

Coherent MIMO radar systems have arguably been the most common subject of study because they can provide finer angular resolution by forming a virtual array with coherent processing based on orthogonal waveforms [8]. Orthogonal waveforms are specifically designed to cooperate with each other and their correlation properties can be used to achieve a desired radiation patterns [9, 10] with a desired antenna gain and angular resolution [11]. In the literature, coherent MIMO waveforms have also been proposed to improve moving target indication (MTI) performance [12].

MIMO radar with non-cooperative radar channels or based on a non-cooperative radar network can also use orthogonal waveforms to mitigate the mutual interference between nodes [13, 14].

An approach used to design orthogonal waveforms is by the formulation of an optimisation problem that accounts for the interference level through a cost function or a constraint. Cost functions have been proposed to minimise the maximum sidelobe level (MSL), the integrated sidelobe level (ISL) or the integrated cross-correlation values between signals [15]. Additional constraints have been proposed to limit the signal energy, provide a constant amplitude and control spectral content [16]. The challenge with optimisation solutions is that an optimal solution is guaranteed to exist only when the problem is convex or can be relaxed to convex [9, 14]. However, often the optimisation is too complex and heuristic methods based on specific classes of waveforms are required. An example of this are those employing polyphase signals [17]. An additional drawback of optimisation methods is they often provide waveforms that are not Doppler tolerant.

In the literature, noise-like stochastic signals have also been used to generate orthogonal waveforms [18, 19]. However, with such signals, controlling the bandwidth and the Doppler tolerance properties is a challenge.

LFM chirps offer good Doppler tolerance, relatively low sidelobes and ease of implementation. They also benefit of quasi orthogonal properties and, as a result, have been previously proposed for use with multi-channel radars [20], MIMO synthetic aperture radar (SAR) [21, 22] and as a possible solution for radar and communication signals coexistence [23]. It is known that up and down-chirps offer a good level of isolation but can only provide two channels. To generate a larger number of channels, combinations of chirp signals with different slopes to form saw-like waveforms have been investigated [24] for MIMO SAR applications. Nevertheless, previous work has largely employed test and try solutions and a rigorous study of the orthogonal properties and limitations of linear chirps with diverse waveform design is missing.

In this paper, MBR systems are introduced as a subclass of MIMO systems. The MBR analytical signal model is derived to show how the cross-channel interference can be mitigated with orthogonal waveforms. An analytical treatment of the orthogonal properties of LFM waveforms is presented. The analytical expression of the cross-ambiguity function between rectangular linear chirps with different bandwidths and different frequency offsets is derived. The derivations are then extended to the case of linear chirps with a Gaussian amplitude modulation. The derived cross-ambiguity functions are used to provide the analytical expressions of the isolation and isolation bound between channels. The analytical results are verified with simulations and experiments at C-band.

2 Multibeam radars

MBR systems generate multiple beams in transmission by means of a linear combination of orthogonal waveforms at each element. Each

beam corresponds to a radar channel and is associated with a specific waveform design to provide a designated functionality. The solution allows the radar to provide multiple simultaneous functions whilst managing radar resources at each channel. Channels are extracted on receive by exploiting the orthogonal properties of the waveforms.

2.1 MBR signal model

We study an MBR radar consisting of an array of K antenna elements each one transmitting a narrowband signal $s_k(t)$, as shown in Fig. 1. The transmitted signals are arranged in a vector

$$\mathbf{s}(t) = [s_1(t)\ s_2(t)\ \cdots\ s_K(t)]^T \tag{1}$$

Let us consider a linear array arrangement and an ideal point target at a distance R from the radar in a direction θ. The signal intercepted by the target is the superposition of phase-shifted delayed replicas of the signals $s_k(t)$ and can be expressed as

$$\hat{s}(t) = \mathbf{a}^T(\theta)\mathbf{s}\left(t - \frac{R}{c}\right)\exp\left(-j2\pi f_c\frac{R}{c}\right) \tag{2}$$

with

$$\mathbf{a}(\theta) = \sqrt{\frac{1}{K}}[a_1(\theta)\ a_2(\theta)\ \cdots\ a_K(\theta)]^T \tag{3}$$

of elements

$$a_k(\theta) = \exp\left(\frac{j2\pi f_c}{c}(k-1)d\sin\theta\right) \tag{4}$$

where f_c is the carrier frequency, c is the speed of light and d is the spacing between antenna elements. Similarly, on receive, each antenna element receives a signal y_k that is a phase-shifted delayed

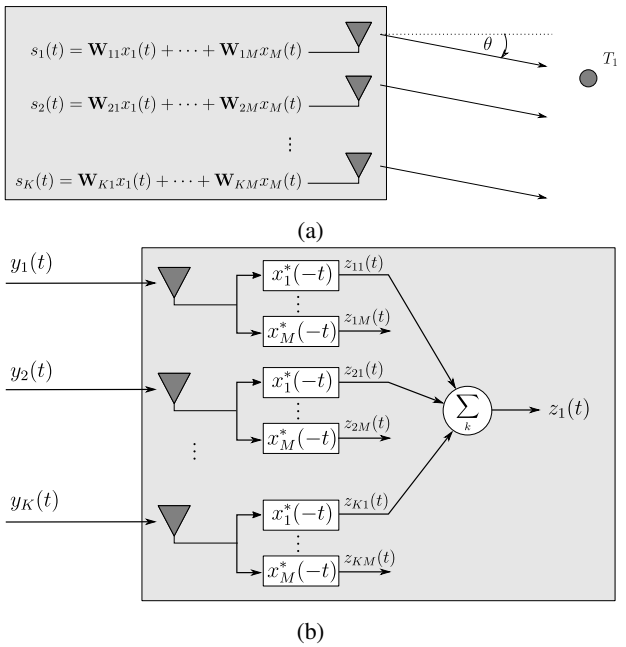

Fig. 1: Schematics of a multibeam radar
a Processing on transmit
b Processing on receive

copy of $\hat{s}(t)$ as

$$y_k = \sqrt{\frac{1}{K}}\exp\left(\frac{j2\pi f_c}{c}(k-1)d\sin\theta\right)\hat{s}\left(t-\frac{R}{c}\right) \times \exp\left(-j2\pi f_c\frac{R}{c}\right) \tag{5}$$

$$= \sqrt{\frac{1}{K}}\exp\left(\frac{j2\pi f_c}{c}(k-1)d\sin\theta\right)\mathbf{a}^T(\theta)\mathbf{s}\left(t-\frac{2R}{c}\right) \times \exp\left(-j2\pi f_c\frac{2R}{c}\right) \tag{6}$$

We define the vector of all received signals

$$\mathbf{y}(t) = [y_1(t)\ y_2(t)\ \cdots\ y_K(t)]^T \tag{7}$$

and note this can be expressed as

$$\mathbf{y}(t) = \gamma\mathbf{b}(\theta)\mathbf{a}^T(\theta)\mathbf{s}\,(t-t_0)\exp\,(-j2\pi f_c t_0) \tag{8}$$

where

$$\mathbf{b}(\theta) = \sqrt{\frac{1}{K}}[b_1(\theta)\ b_2(\theta)\ \cdots\ b_K(\theta)]^T \tag{9}$$

$\gamma \in \mathbb{C}$ is the reflectivity of the target and $t_0 = 2R/c$ is the echo time delay. For a monostatic system

$$b_k(\theta) = a_k(\theta) = \exp\left(\frac{j2\pi f_c}{c}(k-1)d\sin\theta\right) \tag{10}$$

Each element antenna of an MBR transmits a linear combination of M orthogonal waveforms $\mathbf{x}(t)$ (see Fig. 1a) and

$$\mathbf{s}(t) = \mathbf{W}\mathbf{x}(t) \tag{11}$$

where $\mathbf{W}$ is a $K \times M$ steering matrix whose columns are the steering vectors

$$\mathbf{W} = [\mathbf{a}(\tilde{\theta}_1)\ \mathbf{a}(\tilde{\theta}_2)\ \cdots\ \mathbf{a}(\tilde{\theta}_M)] \tag{12}$$

Each element of $\mathbf{x}(t)$ is a waveform $x_m(t)$ that corresponds to a beam pointing in the direction $\tilde{\theta}_m$. If a beam of the MBR points in the direction of the target θ then there will exist a column of $\mathbf{W}$ such that $\mathbf{a}(\tilde{\theta}_m) = \mathbf{a}^*(\theta)$. The received signal vector

$$\mathbf{y}(t) = \alpha\mathbf{b}(\theta)\mathbf{a}^T(\theta)\mathbf{W}\mathbf{x}(t-t_0) \tag{13}$$

with $\alpha = \gamma\exp\,(-j2\pi f_c t_0)$ is processed with a bank of matched filters to separate the beams. Extraction of the mth channel is achieved by matched filtering all signals at each element to $x_m(t)$ before applying a weighting vector $\tilde{\mathbf{b}}$ and summing them together as

$$z_m(t) = \tilde{\mathbf{b}}^T\left[\mathbf{y}(t) * x_m^*(-t)\right] \tag{14}$$

$$= \alpha\tilde{\mathbf{b}}^T\mathbf{b}(\theta)\mathbf{a}^T(\theta)\left[\mathbf{W}\mathbf{x}(t-t_0) * x_m^*(-t)\right] \tag{15}$$

$$= \alpha\tilde{\mathbf{b}}^T\mathbf{b}(\theta)\mathbf{a}^T(\theta)\left[\sum_{k=1}^{K}\mathbf{a}(\tilde{\theta}_k)x_k(t-t_0) * x_m^*(-t)\right] \tag{16}$$

$$= \alpha\tilde{\mathbf{b}}^T\mathbf{b}(\theta)\mathbf{a}^T(\theta)\left[\sum_{k=1}^{K}\mathbf{a}(\tilde{\theta}_k)R_{km}(t-t_0)\right] \tag{17}$$

where $R_{km}(t)$ is the cross-correlation function between x_k and x_m. When no weights are applied on receive $\tilde{\mathbf{b}} = \mathbf{1}_K$ with $\mathbf{1}_K$ being the

$K \times 1$ vector of ones. The received waveform can be expressed as

$$z_m(t) = \alpha \tilde{\mathbf{b}}^T \mathbf{b}(\theta)\mathbf{a}^T(\theta)\mathbf{a}(\tilde{\theta}_m)\mathbf{R}_{mm}(t-t_0) + \alpha \tilde{\mathbf{b}}^T \mathbf{b}(\theta)\mathbf{a}^T(\theta)\left[\sum_{k\neq m} \mathbf{a}(\tilde{\theta}_k)\mathbf{R}_{km}(t-t_0)\right] \quad (18)$$

and finally, considering that all the signals in $\mathbf{x}(t)$ are orthogonal, as

$$z_m(t) = \alpha \tilde{\mathbf{b}}^T \mathbf{b}(\theta)\mathbf{a}^T(\theta)\mathbf{a}(\tilde{\theta}_m)\mathbf{R}_{mm}(t-t_0) \quad (19)$$

This is the typical output of a standard phased array. The advantage is that the MBR transmits different waveform designs in different directions and waveforms can be selected to suit different radar functions and better manage resources. Eq. (18) shows that cross-channel interference components depend on the orthogonal properties of the transmitted waveforms as well as on the steering vectors. This indicates that, for practical applications that require very high levels of isolation, the effects of the limitations of the waveform orthogonal properties on cross-channel interference can be mitigated with the joint use of spatial diversity. Similarly to standard MIMO radars, the orthogonal properties of the transmitted waveforms remain the key driving feature to guarantee very low cross-channel interference.

2.2 Channel isolation

The derivations presented in the previous section show that the interference between different channels is described by the cross-correlation function

$$R_{ij}(\tau) = \int_{-\infty}^{\infty} x_i^*(t)x_j(t+\tau)dt \quad (20)$$

The isolation $I_i(\tau)$ represents the level of isolation of the ith channel with all other channels and is defined as the ratio between the peak of the amplitude of the autocorrelation function and the amplitude of the sum of cross-correlation functions as

$$I_i(\tau) = \left|\frac{R_{ii}(0)}{\sum_{j\neq i} R_{ij}(\tau)}\right| \geq \frac{|R_{ii}(0)|}{\sum_{j\neq i}|R_{ij}(\tau)|} \quad (21)$$

Eq. (21) can be extended to account for the Doppler shift f_D. It can be shown that, in this case, the isolation is a function of the cross-ambiguity function

$$\chi_{ij}(\tau, f_D) = \int_{-\infty}^{\infty} x_i^*(t)x_j(t+\tau)\exp(j2\pi f_D t)dt \quad (22)$$

and is defined as

$$I_i(\tau, f_D) = \left|\frac{\chi_{ii}(0,0)}{\sum_{j\neq i}\chi_{ij}(\tau, f_D)}\right| = \left|\frac{\chi_{ii}(0,0)}{\sum_{j\neq i}\chi^*_{ji}(-\tau, f_D)}\right| \quad (23)$$

and thus

$$I_i(\tau, f_D) \geq \frac{|\chi_{ii}(0,0)|}{\sum_{j\neq i}|\chi_{ij}(\tau, f_D)|} = \left(\sum_{j\neq i}\frac{1}{I_{ij}(\tau, f_D)}\right)^{-1} \quad (24)$$

where

$$I_{ij}(\tau, f_D) = \left|\frac{\chi_{ii}(0,0)}{\chi_{ij}(\tau, f_D)}\right| \quad (25)$$

is the isolation between two channels.

3 Rectangular LFM waveforms

Rectangular LFM waveforms are widely used in radar systems because a constant instantaneous power allows the transmitter to operate in saturation.

3.1 General isolation derivation

Let us consider a multi-channel system, transmitting a combination of linear chirps with the same amplitude A, duration T, bandwidth B_i and frequency offset f_{si}. The complex envelope of each chirp is

$$x_i(t) = A\,\mathrm{rect}\left(\frac{t}{T}\right)\exp\left(2\pi j(f_{si}t + \frac{1}{2}\mu_i t^2)\right) \quad (26)$$

where $\mu_i = B_i/T$ is the chirp rate and

$$\mathrm{rect}\left(\frac{t}{T}\right) = \begin{cases} 1, & t \in \left[-\frac{T}{2}, \frac{T}{2}\right] \\ 0, & \text{otherwise} \end{cases} \quad (27)$$

Because all signals have the same amplitude and the same time duration, they have the same energy $E = A^2T$. We study the isolation properties between two linear chirps, $x_i(t)$ and $x_j(t)$, with different chirp rates, μ_i and μ_j, and different frequency offsets, f_{si} and f_{sj}, to investigate if these can be exploited for waveform diversity. An example of chirps with different bandwidths and different offset frequencies is shown in Fig. 2. The isolation between $x_i(t)$ and $x_j(t)$ is found by replacing the expressions of $x_i(t)$ and $x_j(t)$ in (22) to calculate the cross-ambiguity function as

$$\chi_{ij}(\tau, f_D) = A^2\exp\left(j2\pi(f_{sj}\tau + \frac{1}{2}\mu_j\tau^2 - \frac{(f_{sj}-f_{si}-f_D+\mu_j\tau)^2}{2(\mu_j-\mu_i)})\right) \times \int_{\eta_1}^{\eta_2}\exp\left(j\pi(\mu_j-\mu_i)(t+\frac{f_{sj}-f_{si}-f_D+\mu_j\tau}{\mu_j-\mu_i})^2\right)dt \quad (28)$$

The integration interval $[\eta_1\ \eta_2]$ is a function of τ as

$$[\eta_1\ \eta_2] = \begin{cases} [-\frac{T}{2},\ \frac{T}{2}-\tau], & \tau \in [0, T] \\ [-\frac{T}{2}-\tau,\ \frac{T}{2}], & \tau \in [-T, 0) \end{cases} \quad (29)$$

and is zero for all $|\tau| > T$. Assuming with no loss of generality that $\mu_j > \mu_i$ and $\mu_j > 0$, Eq. (28) can be further simplified with the change of variables

$$\xi = \sqrt{2(\mu_j-\mu_i)}\left(t + \frac{f_{sj}-f_{si}-f_D+\mu_j\tau}{\mu_j-\mu_i}\right) \quad (30)$$

$$d\xi = \sqrt{2(\mu_j-\mu_i)}\,dt \quad (31)$$

to obtain

$$\chi_{ij}(\tau, f_D) = A^2K(\tau, f_D)\int_{\xi(\eta_1)}^{\xi(\eta_2)}\exp\left(j\frac{\pi}{2}\xi^2\right)d\xi \quad (32)$$

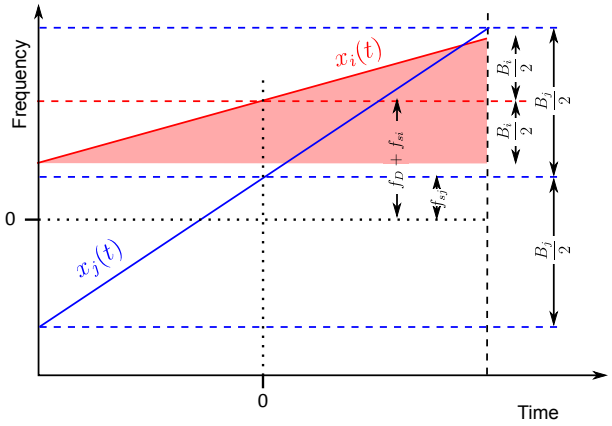

Fig. 2: Time-frequency diagram of two LFM signals

with

$$K(\tau, f_D) = \frac{\exp\left(j\pi\left(2f_{sj}\tau + \mu_j\tau^2 - \frac{(f_{sj}-f_{si}-f_D+\mu_j\tau)^2}{\mu_j-\mu_i}\right)\right)}{\sqrt{2(\mu_j-\mu_i)}} \quad (33)$$

Noting that the integral in Eq. (32) is the difference between two complex Fresnel integrals

$$F(\alpha) = \int_0^\alpha \exp\left(j\frac{\pi}{2}\xi^2\right) d\xi \quad (34)$$

the final expression of the cross-ambiguity function becomes

$$\chi_{ij}(\tau, f_D) = A^2 K(\tau, f_D)\Big(F(\xi(\eta_2)) - F(\xi(\eta_1))\Big) \quad (35)$$

In the above equation, for $0 \leq \tau \leq T$

$$\xi(\eta_1) = \sqrt{2(\mu_j-\mu_i)}\left(-\frac{T}{2} + \frac{f_{sj}-f_{si}-f_D}{\mu_j-\mu_i} + \frac{\mu_j\tau}{\mu_j-\mu_i}\right) \quad (36)$$

$$\xi(\eta_2) = \sqrt{2(\mu_j-\mu_i)}\left(\frac{T}{2} + \frac{f_{sj}-f_{si}-f_D}{\mu_j-\mu_i} + \frac{\mu_i\tau}{\mu_j-\mu_i}\right) \quad (37)$$

and for $-T \leq \tau < 0$

$$\xi(\eta_1) = \sqrt{2(\mu_j-\mu_i)}\left(-\frac{T}{2} + \frac{f_{sj}-f_{si}-f_D}{\mu_j-\mu_i} + \frac{\mu_i\tau}{\mu_j-\mu_i}\right) \quad (38)$$

$$\xi(\eta_2) = \sqrt{2(\mu_j-\mu_i)}\left(\frac{T}{2} + \frac{f_{sj}-f_{si}-f_D}{\mu_j-\mu_i} + \frac{\mu_j\tau}{\mu_j-\mu_i}\right) \quad (39)$$

By replacing Eq. (35) in (25), with $\Delta B = B_j - B_i$, $f_{sj} = 0$ Hz, and noting that $\chi_{ii}(0,0) = E = A^2T$, the expression of the isolation for $|\tau| \leq T$ can be written as

$$I_{ij}(\tau, f_D)\Big|_{\tau<0} = \sqrt{2T\Delta B}\left|F\left(\sqrt{\frac{2\Delta B}{T}}\left(\frac{T}{2} + \frac{B_j\tau - T(f_{si}+f_D)}{\Delta B}\right)\right) - F\left(\sqrt{\frac{2\Delta B}{T}}\left(-\frac{T}{2} + \frac{B_i\tau - T(f_{si}+f_D)}{\Delta B}\right)\right)\right|^{-1} \quad (40)$$

and

$$I_{ij}(\tau, f_D)\Big|_{\tau\geq0} = \sqrt{2T\Delta B}\left|F\left(\sqrt{\frac{2\Delta B}{T}}\left(-\frac{T}{2} + \frac{B_j\tau - T(f_{si}+f_D)}{\Delta B}\right)\right) - F\left(\sqrt{\frac{2\Delta B}{T}}\left(\frac{T}{2} + \frac{B_i\tau - T(f_{si}+f_D)}{\Delta B}\right)\right)\right|^{-1} \quad (41)$$

It is also worth observing that $B_i > 0$ for up-chirps and $B_i < 0$ for down-chirps and ΔB changes accordingly. The results are in agreement with those presented in [25] for the case with no Doppler shift.

Note that the isolation is symmetric when $f_{si} = f_{sj} = f_D = 0$ Hz and can be simplified as

$$I_{ij}(\tau, 0) = \sqrt{2T\Delta B}\left|F\left(\sqrt{\frac{2\Delta B}{T}}\left(-\frac{T}{2} + \frac{B_j|\tau|}{\Delta B}\right)\right) - F\left(\sqrt{\frac{2\Delta B}{T}}\left(\frac{T}{2} + \frac{B_i|\tau|}{\Delta B}\right)\right)\right|^{-1} \quad (42)$$

3.2 Upper cross-ambiguity bound

In this section, a bound of the maximum value of the cross-ambiguity function in (35) is determined, to obtain the lower bound of the isolation for rectangular chirps. To do this, we note that the amplitude of the cross-ambiguity function can be expressed as a function of the amplitude of the difference between two Fresnel integrals as

$$|\chi_{ij}(\tau, f_D)| = \sqrt{\frac{T}{2\Delta B}}A^2\big|C(\xi(\eta_2)) + jS(\xi(\eta_2)) - C(\xi(\eta_1)) - jS(\xi(\eta_1))\big| \quad (43)$$

where $C(\cdot)$ and $S(\cdot)$ are the real and imaginary parts of $F(\cdot)$. An upper bound of the amplitude of the cross-ambiguity function can be expressed with the following inequality

$$|\chi_{ij}(\tau, f_D)| \leqslant \sqrt{\frac{T}{2\Delta B}}A^2\Big[\big|C(\xi(\eta_2)) + jS(\xi(\eta_2))\big| + \big|C(\xi(\eta_1)) + jS(\xi(\eta_1))\big|\Big] \quad (44)$$

Noting that the amplitude of the Fresnel integral admits an upper bound $|F(\alpha)| < F_{max} \approx 0.9491$, the inequality can be further expressed as

$$|\chi_{ij}(\tau, f_D)| \leqslant \sqrt{\frac{T}{2\Delta B}}A^2\left[F_{max} + F_{max}\right] \quad (45)$$

and therefore the isolation

$$I_{ij}(\tau, f_D) = \left|\frac{\chi_{ii}(0,0)}{\chi_{ij}(\tau, f_D)}\right| \quad (46)$$

$$\geq \frac{A^2T}{2\sqrt{\frac{T}{2\Delta B}}A^2F_{max}} \quad (47)$$

$$> \sqrt{\frac{T\Delta B}{2}} \quad (48)$$

This is a key result that indicates that the lower bound of the isolation is proportional to the square root of the pulse width and the difference between the bandwidths of the waveforms

$$(I_{ij})_{min} \propto \sqrt{T\Delta B} \quad (49)$$

3.3 Up-chirp and down-chirp orthogonality

A special case of LFM signal orthogonality is the combination of an up-chirp and a down-chirp, with the same bandwidth and opposite chirp rates $\mu = \mu_j = -\mu_i$ with $\mu = B/T$. When there is no Doppler effect $f_D = 0$ Hz, and the offset frequencies are $f_{si} = f_{sj} = 0$ Hz, the magnitude of the cross-correlation function can be

expressed from Eq. (35) as

$$|R_{ij}(\tau)| = A^2\sqrt{\frac{T}{B}}\left|F\left(\sqrt{BT}\left(1-\frac{|\tau|}{T}\right)\right)\right| \tag{50}$$

which corresponds to a known result available in [26]. Using the limits of the complex Fresnel integral

$$\lim_{\alpha\to\infty}|F(\alpha)| = \lim_{\alpha\to\infty}|C(\alpha)+jS(\alpha)| = \sqrt{1/2} \tag{51}$$

the isolation can then be approximated for $BT \gg 1$ as

$$I_{ij} \approx T\sqrt{\frac{2B}{T}} = \sqrt{2BT} \tag{52}$$

This result, together with those in Eq. (48) and Eq. (52), corroborates the results in [15] which found that waveform orthogonality approximately improves with the square root of the time-bandwidth product.

3.4 Simulation results

This section presents the simulation results carried out to verify the orthogonal properties of rectangular linear chirps derived in Section 3.1. The case for two up-chirps with different bandwidths $B_j = B_i + \Delta B$ and hence different chirp slopes is shown in Fig. 3a. The results are relative to two LFM signals with the same time duration $T = 10\ \mu$s and the same offset frequencies $f_{si} = f_{sj} = 0$ MHz. The bandwidth B_j is fixed to 50 MHz and B_i is varied by subtracting ΔB from B_j. A graphical representation of the resulting frequency modulations is depicted in Fig. 2. The range cut of the ambiguity function, that is the cross-correlation R_{ij}, is plotted in Fig. 3a.

The results in the figure show that the bigger the bandwidth difference ΔB, the better suppression of the second channel. Increasing ΔB results in longer sidelobes that extend towards negative and positive delays. This behaviour can be explained by examining Eq. (21) and the time-frequency modulation in Fig. 2. For positive time delays, $x_i(t)$ moves to the left in the time-frequency plot until there is no overlapping with $x_j(t)$. This causes energy decoupling in the time-frequency domain which results in reduced channel interference, hence the drop in cross-correlation. Energy coupling can be similarly explained for the positive delays. To investigate the isolation level as a function of bandwidth difference, B_j is fixed to 50 MHz and $\Delta B = B_j - |B_i|$ was varied. The corresponding isolation levels are shown in Fig. 3b. Results show that the signal combination of up-chirp and down-chirp results in better performance when compared to a pair of chirps with slope of the same sign, that is a pair of up-chirps or a pair of down-chirps. Additionally, the isolation lower bound is correctly predicted by Eq. (47).

Waveform orthogonality was also analysed for up-chirps with a different offset frequency. To test this, the bandwidths were fixed

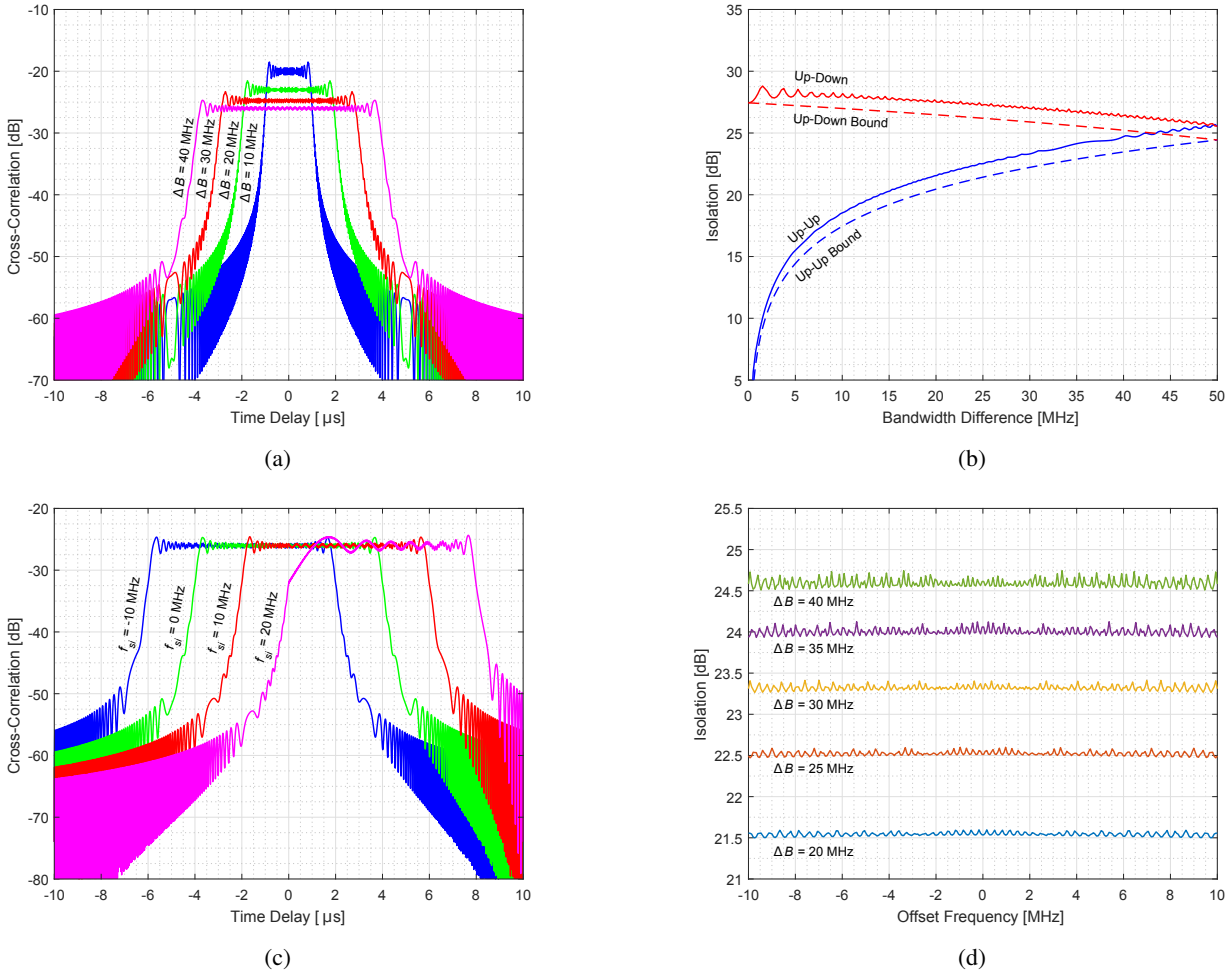

Fig. 3: Simulated results for two LFM chirp signals
a Amplitude of the cross-correlation between signals with different bandwidths
b Isolation between a pair of LFM signals as a function of bandwidth difference
c Amplitude of the cross-correlation between signals with different offset frequencies
d Isolation between a pair of LFM signals as a function of offset frequency

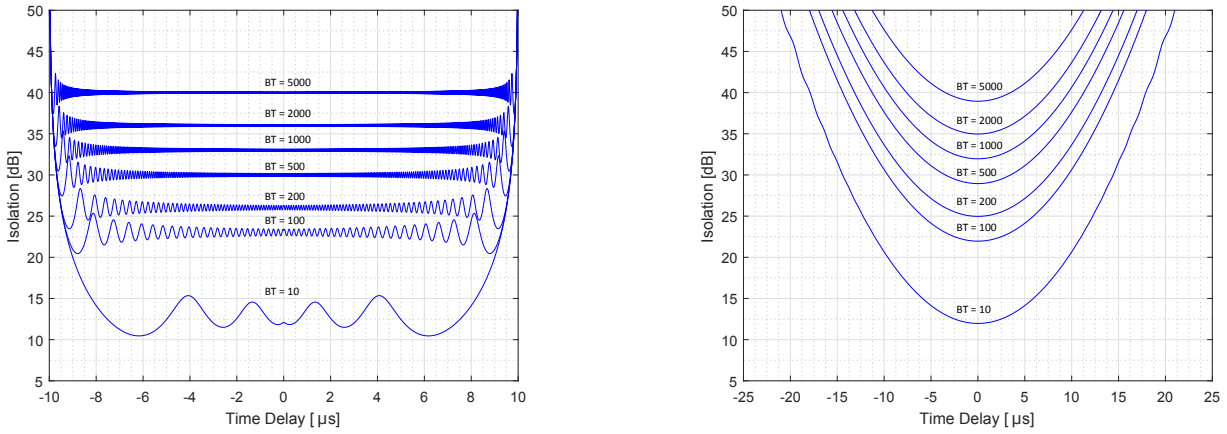

(a) (b)

Fig. 4: Simulated isolation of up-chirp and down-chirp signals with equal bandwidth and fixed time duration
a Rectangular LFM signal
b Gaussian LFM signal

to $B_j = 50$ MHz and $B_i = 10$ MHz, and the offset frequency f_{si} was varied for a set of values as indicated in Fig. 3c. The results of this analysis relate to the Doppler tolerance properties of the cross-ambiguity function. As discussed for the previous case, varying the offset frequency of $x_i(t)$ results in a shift of the modulation curve up and down in time-frequency domain, as can be seen in Fig. 2. Therefore, increasing the offset frequency has a similar effect as moving the cross-correlation curve to the right and this does not affect the isolation properties. The frequency shift invariance is depicted in Fig. 3d where the isolation is plotted according to (21) as a function of the bandwidth difference ΔB, where $B_j = 50$ MHz is fixed. Increasing ΔB from 20 MHz to 40 MHz improves the isolation from 21.5 dB to 24.6 dB. Additionally, when $B_i = 20$ MHz, all the isolation values remain at about 23.3 dB.

Finally, a comparison of the isolation performance for different time-bandwidth products was carried out. Fig. 4a shows the isolation as a function of time for two chirps of the same time duration $T = 10$ μs but opposite chirp rates for a range of time-bandwidth products. Results show that isolation improves of about 25 dB from $BT = 10$ to $BT = 5000$, corroborating the theoretical results that the isolation increases when the time-bandwidth product increases.

4 Gaussian LFM waveforms

In this section, the orthogonal properties of Gaussian amplitude modulated LFM waveforms are investigated. As for the linear chirp, a general expression of the isolation will be derived to investigate orthogonality properties between chirps of the same duration but with different linear frequency modulation designs. A study of the special case of up-chirps and down-chirps is also presented.

4.1 General isolation derivation

Let us consider a multi-channel system transmitting a combination of Gaussian LFM chirps with unit energy of the form

$$x_i(t) = \left(\frac{1}{\pi\lambda^2}\right)^{1/4} \exp\left(-\frac{t^2}{2\lambda^2} + j\left(a_i t + b_i t^2\right)\right) \tag{53}$$

where $T = 2\lambda$ is the pulse duration and $b_i = \pi B_i/T$ determines the frequency slope of the chirp with bandwidth B_i. The signal model follows the definition available in [27] except for the component that depends on $a_i = 2\pi f_{si}$ which represents the frequency offset f_{si} of the chirp at $t = 0$.
To derive the isolation between Gaussian chirps with different bandwidths and offset frequencies, the cross-ambiguity function is calculated from the definition in (22). The detailed calculations are presented in the Appendix and provide the final result

$$\chi_{ij}(\tau, f_D) = \sqrt{\frac{1}{\alpha\lambda^2}} \exp\left(j(b_j\tau^2 + a_j\tau) - \frac{\tau^2}{2\lambda^2} + \frac{\beta^2}{4\alpha}\right) \tag{54}$$

where

$$\alpha = \frac{1}{\lambda^2} - j(b_j - b_i) \tag{55}$$

and

$$\beta = \frac{\tau}{\lambda^2} + j(a_i - a_j - 2\pi f_D - 2b_j\tau) \tag{56}$$

The amplitude of the cross-ambiguity function can be expressed as

$$|\chi_{ij}(\tau, f_D)| = \sqrt{\frac{1}{\lambda^2}} \exp\left(-\frac{\tau^2}{2\lambda^2}\right) \left|\sqrt{\frac{1}{\alpha}} \exp\left(\frac{\beta^2}{4\alpha}\right)\right| \tag{57}$$

It can be verified that for $a_i = a_j$ and $b_i = b_j$ the amplitude of the cross-ambiguity function is

$$|\chi_{ii}(\tau, f_D)| = \exp\left(-\frac{\tau^2}{4\lambda^2} - \pi^2\lambda^2\left(f_D + \frac{b_i\tau}{\pi}\right)^2\right) \tag{58}$$

and, as expected, this coincides with the analytical solution of the ambiguity function of the Gaussian chirp available in [27].
Following Eq. (57) the general expression of the isolation can be expressed as

$$I(\tau, f_D) = \lambda \exp\left(\frac{\tau^2}{2\lambda^2}\right) \left|\sqrt{\frac{1}{\alpha}} \exp\left(\frac{\beta^2}{4\alpha}\right)\right|^{-1} \tag{59}$$

For $f_D = 0$ and $a_i = a_j$, Eq. (54) corresponds to the cross-correlation between two Gaussian up-chirps with the same offset frequency. In this case,

$$\alpha = \frac{1}{\lambda^2}\left[1 - j\lambda^2(b_j - b_i)\right] \tag{60}$$

$$\beta = \frac{\tau}{\lambda^2}\left[1 - j2\lambda^2 b_j\right] \tag{61}$$

and the cross-correlation becomes

$$R_{ij}(\tau) = \frac{\exp\left(\frac{\left(1+2jb_i\lambda^2\right)\left(j+2b_j\lambda^2\right)\tau^2}{4\lambda^2\left(\lambda^2(b_i-b_j)-j\right)}\right)}{\sqrt{1 + j\lambda^2(b_i - b_j)}} \tag{62}$$

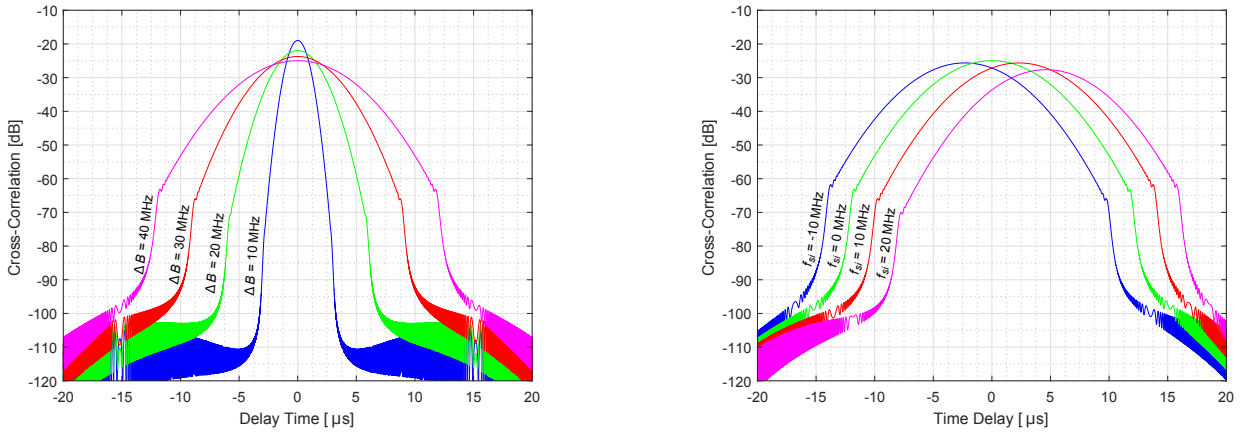

(a) (b)

Fig. 5: Simulated amplitude of the cross-correlation between Gaussian up-chirp signals
a Different bandwidths
b Different offset frequencies

4.2 Up-chirp and down-chirp orthogonality

In this section, we derive the cross-correlation between a Gaussian up-chirp and a Gaussian down-chirp with the same bandwidth and opposite slope ($b = b_i = -b_j$ and $a_i = a_j$). In this case,

$$\alpha = \frac{1}{\lambda^2} + j2b \tag{63}$$

$$\beta = \tau\alpha \tag{64}$$

and (62) can be simplified to

$$R_{ij}(\tau) = \sqrt{\frac{1}{1+j2b\lambda^2}}\ \exp\left(-\frac{\tau^2}{4}\left(\frac{1}{\lambda^2} + j2b\right)\right) \tag{65}$$

As a result, the isolation between a Gaussian up-chirp and a Gaussian down-chirp is

$$I_{ij}(\tau) = \left|\sqrt{1+j2b_i\lambda^2}\ \exp\left(\frac{\tau^2}{4}\left(\frac{1}{\lambda^2} + 2jb\right)\right)\right| \tag{66}$$

$$= \sqrt[4]{1+4b^2\lambda^4}\ \exp\left(\frac{\tau^2}{4\lambda^2}\right) \tag{67}$$

The minimum of the isolation occurs for $\tau = 0$ and is

$$(I_{ij})_{min} = \sqrt[4]{1+4b^2\lambda^4} \tag{68}$$

Finally, the isolation lower bound can be expressed as a function of B and T as

$$(I_{ij})_{min} = \sqrt[4]{1+\frac{\pi^2B^2T^2}{4}} \tag{69}$$

and for $BT \gg 1$ can be approximated with

$$(I_{ij})_{min} \approx \sqrt{\frac{\pi}{2}BT} \tag{70}$$

Eq. (70) corroborates that the isolation increases approximately as a square root of the time-bandwidth product.

4.3 Simulation results

Simulations were carried out to investigate the cross-correlation and isolation properties of the Gaussian chirp. Fig. 5a shows the cross-correlation between two Gaussian chirps as a function of time and for different values of ΔB, for $f_{sj} = f_{si} = 0$ MHz, $f_D = 0$ and $B_j = 50$ MHz. Results show that, as expected, the peak of the cross-correlation decreases when ΔB increases. They also show that the peak values are lower than that of constant envelope linear chirps given the same ΔB. The effect of varying the offset frequency f_{si} on the cross-correlation properties is studied in Fig. 5b for two up-chirps with $\Delta B = 40$ MHz and $f_{sj} = 0$. Results show that the isolation properties of Gaussian chirps are not invariant with respect to the offset frequency and this is due to the amplitude tapering. Signal with $f_{si} = 0$ MHz has a maximum cross-correlation value because, in this case, the spectrum peaks of both signals i and j are aligned in the frequency domain. Fig. 4b shows the isolation results for the Gaussian up-chirp and down-chirp signals with the same bandwidth. Results show that the isolation values agree with the analytical expression in (69).

4.4 Comparison of the rectangular and Gaussian AM

This section presents a comparison between rectangular and Gaussian chirps based on the simulation results. Isolation performance for up and down-chirp signals with the same bandwidth is presented in Table 1. The table shows the minimum values of the isolation curves in Fig. 4a and Fig. 4b. The results in the table show that the Gaussian chirp on average offer slightly better isolation than the rectangular chirp. However, the rectangular chirp has the advantage of allowing transmissions in saturation mode.

Table 1 Simulated isolation for up-chirp and down-chirp signal pairs

BT Product	Rectangular	Gaussian
10	10.45 dB	11.97 dB
100	20.45 dB	21.96 dB
200	23.46 dB	24.97 dB
500	27.44 dB	28.95 dB
1000	30.45 dB	31.96 dB
2000	33.46 dB	34.97 dB
5000	37.44 dB	38.95 dB

The isolation performance are further compared in Fig. 6 for the case with $B_j = 50$ MHz and $\Delta B = B_j - |B_i| = 25$ MHz. Results show the isolation of the Gaussian chirp is about ~ 0.5 dB higher than that of the linear chirp although the sidelobes of the Gaussian chirp are extended. A further improvement can be achieved when the chirp rate of the signal with the smaller bandwidth $B_i = 25$ MHz has opposite sign. Fig. 6 shows that, with

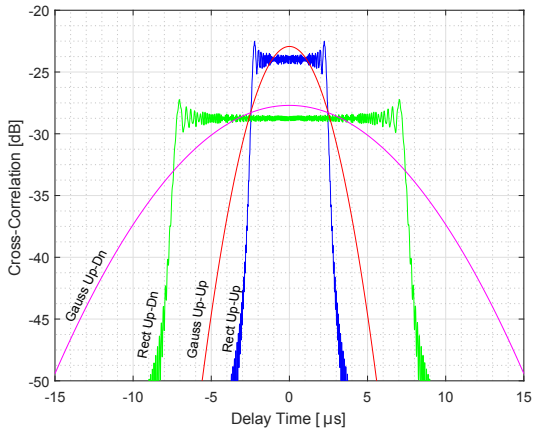

Fig. 6: Comparison between cross-correlation functions

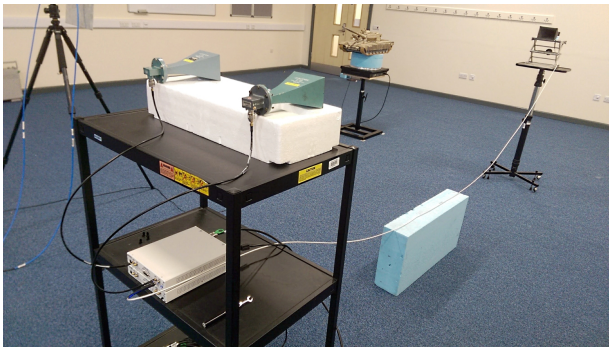

Fig. 7: Photo of the experimental setup

such combination, an improvement of approximately ~ 5 dB can be achieved.

5 Experimental results

Experiments were carried out to confirm the simulation results with real data and to test the detection performance of the proposed waveforms for a rotating target with a two channel range-Doppler map.

5.1 Analysis of orthogonal properties

The measurement setup consisted of a universal software radio peripheral (USRP) device connected to two identical transmitting horn antennas and a receiving antenna placed at a distance of 4 m from the transmitter. Orthogonal waveforms, one for each transmitting horn, were transmitted and received with the receiving antenna. Fig. 7 shows a photo of the experimental setup.

Signals were generated with a carrier frequency $f_c = 6.0$ GHz and the received signals were sampled at a rate of $f_s = 125$ MHz. The transmitted waveform parameters were selected to match the simulations with a waveform duration of $T = 10$ μs and because the setup was stationary with $f_D = 0$. Fig. 8a shows the cross-correlation results for a pair of rectangular linear up-chirps as a function of time for different ΔB. The results are relative to the case with $B_j = 50$ MHz and $f_{sj} = f_{si} = 0$ MHz. The experimental results are in agreement with those of the simulations. Fig. 8b shows the output of the filter matched to $x_j(t)$, when a pair of waveforms was transmitted simultaneously, for $B_j = 50$ MHz, $f_{sj} = 25$ MHz, $B_i = 20$ MHz and $f_{si} = 20$ MHz. Results show the isolation reached a value $I_{ji} = 20$ dB and this corroborates the simulation results. The effects of the bandwidth offset and of the pulse duration on the isolation performance for combinations of up and down-chirps are shown in Table 2, where $\Delta B = B_j - |B_i|$. Results show that increasing the time duration T and the bandwidth difference improves the isolation. Additionally, results show that the combination of chirps with slopes of opposite sign performs better when compared to pairs of up-chirps or down-chirps.

Table 2 Measured isolation for rectangular LFM waveforms

T	Chirp	$\Delta B =$ 10 MHz	$\Delta B =$ 20 MHz	$\Delta B =$ 30 MHz	$\Delta B =$ 40 MHz
10 μs	Up-Up	16.90 dB	20.32 dB	22.65 dB	23.46 dB
10 μs	Up-Down	26.32 dB	26.86 dB	25.86 dB	25.67 dB
20 μs	Up-Up	19.85 dB	23.59 dB	25.63 dB	26.67 dB
20 μs	Up-Down	29.31 dB	29.82 dB	29.11 dB	28.47 dB

Additional experiments were carried out to compare the performance between rectangular and Gaussian LFM signals. For these measurements, the sampling frequency was set to $f_s = 75$ MHz and $T = 10$ μs. The bandwidth of the signal $x_j(t)$ was fixed to $B_j = 10$ MHz and the bandwidth of $x_i(t)$, $B_i = |B_j - \Delta B|$, was varied as indicated in Table 3. It can be observed that the Gaussian LFM performs better than the rectangular modulation. Isolation is increasing with the time-bandwidth product if both signals have increasing

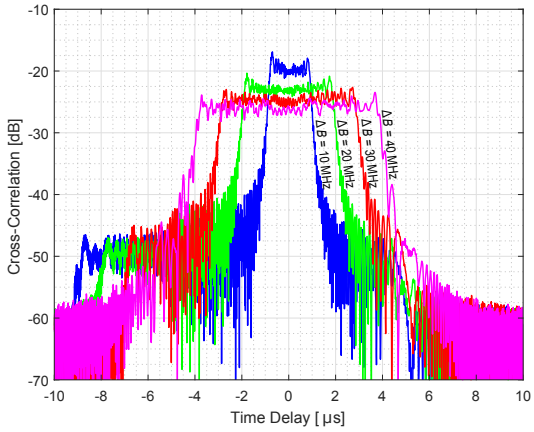

(a)

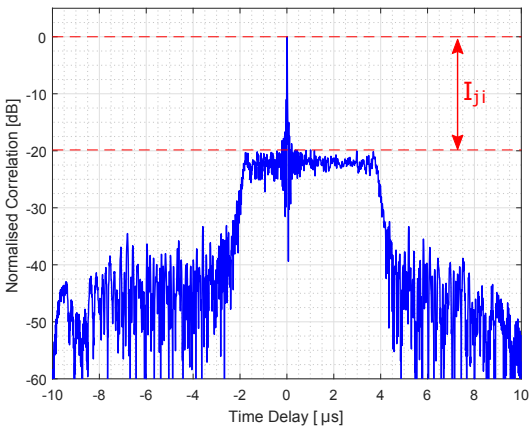

(b)

Fig. 8: Experimental results for rectangular LFM signals
a Amplitude of the cross-correlation between up-chirps with different bandwidths
b Response of the matched filter in the presence of an orthogonal interfering LFM signal

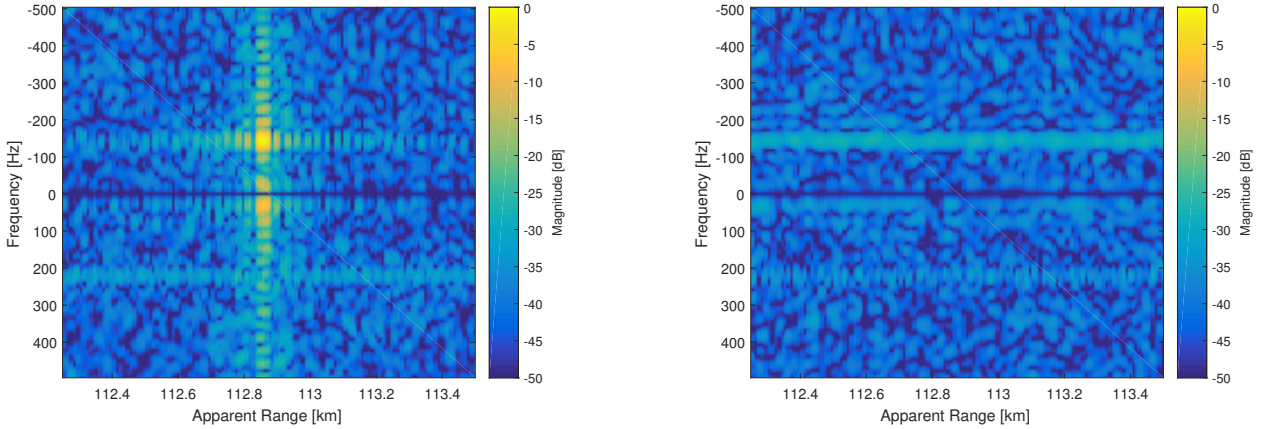

Fig. 9: Experimental two-channel range-Doppler maps relative to rectangular LFM signals
a Co-channel response to target
b Adjacent channel response to target

chirp rates. In the case of up-chirp and down-chirp, $\Delta B = B_j - |B_i|$ does not have a significant impact on the isolation.

Table 3 Measured isolation for rectangular and Gaussian chirp signals

Type	Chirp	$\Delta B =$ 2 MHz	$\Delta B =$ 4 MHz	$\Delta B =$ 6 MHz	$\Delta B =$ 8 MHz
Rect	Up-Up	11.23 dB	14.12 dB	15.78 dB	16.63 dB
Rect	Up-Down	20.74 dB	20.13 dB	19.58 dB	18.83 dB
Gauss	Up-Up	11.91 dB	14.93 dB	16.69 dB	17.89 dB
Gauss	Up-Down	21.39 dB	20.93 dB	20.31 dB	19.66 dB

5.2 Demonstration with a rotating target

In this experiment, data was collected to generate the monostatic range-Doppler map of a rotating target when two orthogonal waveforms were transmitted. A train of pulses was transmitted with an Anritsu signal vector analyser (MS2691A) and target echoes were measured with the receiving channel of the USRP (NI 2943). The target consisted of four rotating blades positioned 4 m away from the radar. Data was collected for a carrier frequency $f_c = 5.0$ GHz and a sampling rate $f_s = 15$ MHz. The transmitted waveforms were an up and down rectangular chirps with $T = 100$ μs, bandwidth $B = 5$ MHz, and pulse repetition frequency $PRF = 1$ kHz. The range-Doppler map was obtained by integrating 30 pulses. On receive, a matched filter to the up-chirp was used to detect the target response and to suppress the echo originated by the down-chirp. The normalised results are shown in Fig. 9a in a dB scale and they indicate the rotating target can be clearly detected. Because the transmitter and the receiver were independent modules and could not be synchronised, the x-axis represents only the apparent range of the target but corroborates the expected range and Doppler resolutions were achieved. The suppression performance of the unmatched signal is shown in Fig. 9b. To produce this figure, only the train of down-chirps was transmitted and processing was achieved with the filter matched to the up-chirp signal. The maximum value of the suppressed channel amounts to -26 dB which agrees with the isolation figure in Table 1 for a signal with $BT = 500$. Due to the limited number of available transmitting elements, in this experiment, the isolation is only provided by the properties of the waveforms. Increasing the number of transmitting elements would allow beamforming and lead to a further improvement of the results.

6 Conclusion

In this paper, MBR systems have been introduced as a solution to provide multiple radar functions by generating multiple channels and multiple independent beams based on waveform diversity. The MBR analytical signal model has been presented to show that the cross-channel interference can be mitigated by transmitting a linear combination of orthogonal waveforms.

The analytical expressions of the cross-ambiguity function between LFM signals with different bandwidths and different frequency offsets have been derived for linear chirps with a rectangular and a Gaussian amplitude modulation. These have been used to calculate the analytical expressions and the lower bounds of the isolation between channels. The analytical results have been verified with simulations as well as with experiments at C-band using a real target.

7 Acknowledgements

The authors would like to express their gratitude to Professor Alfonso Farina for his useful comments. They thank the MCM-ITP programme and Thales Optronique SAS for funding this research.

8 References

1 Griffiths, H.: 'Multistatic, MIMO and networked radar: The future of radar sensors?', *Radar Conference (EuRAD), 2010 European*, 2010, (October), pp. 81–84
2 Li, J., Stoica, P.: 'MIMO Radar with Colocated Antennas', *IEEE Signal Processing Magazine*, 2007, **24**, (5), pp. 106–114
3 Davis, M., Showman, G., Lanterman, A.: 'Coherent MIMO radar: The phased array and orthogonal waveforms', *IEEE Aerospace and Electronic Systems Magazine*, 2014, **29**, (8), pp. 76–91
4 Haimovich, A., Blum, R., Cimini, L.: 'MIMO Radar with Widely Separated Antennas', *IEEE Signal Processing Magazine*, 2008, **25**, (1), pp. 116–129
5 Liu, S., Zhang, Z., Yu, W.: 'A Space-Time Coding Scheme With Time and Frequency Comb-Like Chirp Waveforms for MIMO-SAR', *IEEE Journal of Selected Topics in Signal Processing*, 2017, **11**, (2), pp. 391–403
6 Li, H., Zhao, Y., Cheng, Z., Feng, D.: 'OFDM Chirp Waveform Diversity Design With Correlation Interference Suppression for MIMO Radar', *IEEE Geoscience and Remote Sensing Letters*, 2017, **14**, (7), pp. 1032–1036
7 Xia, X.g., Zhang, T., Kong, L.: 'MIMO OFDM radar IRCI free range reconstruction with sufficient cyclic prefix', *IEEE Transactions on Aerospace and Electronic Systems*, 2015, **51**, (3), pp. 2276–2293
8 Li, J., Stoica, P.: 'MIMO Radar Signal Processing', *John Wiley & Sons, Hoboken, New Jersey*, 2009
9 Fuhrmann, D.R., San Antonio, G.: 'Transmit Beamforming for MIMO radar systems using signal cross-correlation', *IEEE Transactions on Aerospace and Electronic Systems*, 2008, **44**, (1), pp. 171–186
10 Imani, S., Nayebi, M.M., Ghorashi, S.A.: 'Transmit Signal Design in Colocated MIMO Radar Without Covariance Matrix Optimization', *IEEE Transactions on Aerospace and Electronic Systems*, 2017, **53**, (5), pp. 2178–2186

11 Wu, X.H., Kishk, A.A., Glisson, A.W.: 'MIMO-OFDM radar for direction estimation', *IET Radar, Sonar & Navigation*, 2010, **4**, (1), pp. 28
12 Chen, P., Zheng, L., Wang, X., Li, H., Wu, L.: 'Moving Target Detection Using Colocated MIMO Radar on Multiple Distributed Moving Platforms', *IEEE Transactions on Signal Processing*, 2017, **65**, (17), pp. 4670–4683
13 De Nicola, S., De Maio, A., Farina, A., Wicks, M.C.: 'Fast code design for sensors in noncooperative networks', *2010 European Wireless Conference, EW 2010*, 2010, pp. 758–765
14 Gini, F., Maio, A.D., Patton, L.K.: 'Waveform Design and Diversity for Advanced Radar Systems', *IET, London*, 2012, p. 500
15 Monte, L.L., Corigliano, T.A., Himed, B., Baker, C.J.: 'Dynamic range considerations in code division multiple input multiple output radar', *IET Radar, Sonar & Navigation*, 2016, **10**, (8), pp. 1375–1383
16 Aubry, A., De Maio, A., Piezzo, M., Farina, A.: 'Radar waveform design in a spectrally crowded environment via nonconvex quadratic optimization', *IEEE Transactions on Aerospace and Electronic Systems*, 2014, **50**, (2), pp. 1138–1152
17 Deng, H.: 'Polyphase Code Design for Orthogonal Netted Radar Systems', *IEEE Transactions on Signal Processing*, 2004, **52**, (11), pp. 3126–3135
18 Govoni, M.A., Li, H., Kosinski, J.A.: 'Low Probability of Interception of an Advanced Noise Radar Waveform with Linear-FM', *IEEE Transactions on Aerospace and Electronic Systems*, 2013, **49**, (2), pp. 1351–1356
19 Kulpa, K.: 'Signal Processing in Noise Waveform Radar', *Artech House, Artech House, Norwood, Massachusetts*, 2013, p. 269
20 Galati, G., Pavan, G.: 'Orthogonal and Complementary Radar Signals for Multichannel Applications', *2011 8th European Radar Conference*, 2011, (October), pp. 178–181
21 Wang, W.Q., Cai, J.: 'MIMO SAR using Chirp Diverse Waveform for Wide-Swath Remote Sensing', *IEEE Transactions on Aerospace and Electronic Systems*, 2012, **48**, (4), pp. 3171–3185
22 Wang, W.Q.: 'MIMO SAR Chirp Modulation Diversity Waveform Design', *IEEE Geoscience and Remote Sensing Letters*, 2014, **11**, (9), pp. 1644–1648
23 Kota, J., Jacyna, G., Papandreou.Suppappola, A.: 'Nonstationary Signal Design for Coexisting Radar and Communications Systems', *2016 50th Asilomar Conference on Signals, Systems and Computers*, 2016, (3), pp. 549–553
24 Wen-Qin Wang: 'Large Time-Bandwidth Product MIMO Radar Waveform Design Based on Chirp Rate Diversity', *IEEE Sensors Journal*, 2015, **15**, (2), pp. 1027–1034
25 Kocjancic, L., Balleri, A., Merlet, T.: 'Study of the Frequency Slope Effect on the Chirp Waveform Orthogonality', *The IET International Conference on Radar Systems*, 2017
26 Galati, G., Pavan, G.: 'Waveforms Design for Modern and MIMO Radar', 2013, (July), pp. 508–513
27 Cook, C.E., Bernfeld, M.: 'Radar signals: an introduction to theory and application', *Artech House, Boston*, 1993

9 Appendix

The calculations start by applying the definition of cross-ambiguity function as

$$\chi_{ij}(\tau, f_D) = \sqrt{\frac{1}{\pi\lambda^2}} \int_{-\infty}^{\infty} \exp\left(-\frac{t^2}{2\lambda^2} - ja_i t - jb_i t^2\right) \times \exp\left(-\frac{(t+\tau)^2}{2\lambda^2} + ja_j(t+\tau) + jb_j(t+\tau)^2 + j2\pi f_D t\right) dt \quad (71)$$

and by taking out of the integral all the terms that are not a function of t.

$$\chi_{ij}(\tau, f_D) = \sqrt{\frac{1}{\pi\lambda^2}} \exp\left(j(b_j\tau^2 + a_j\tau) - \frac{\tau^2}{2\lambda^2}\right) \times \int_{-\infty}^{\infty} \exp\left(-\left[\frac{1}{\lambda^2} - j(b_j - b_i)\right] t^2\right) \times \exp\left(-\left[\frac{\tau}{\lambda^2} + j(a_i - a_j - 2\pi f_D - 2b_j\tau)\right] t\right) dt \quad (72)$$

We then define

$$\alpha = \frac{1}{\lambda^2} - j(b_j - b_i) \quad (73)$$

$$\beta = \frac{\tau}{\lambda^2} + j(a_i - a_j - 2\pi f_D - 2b_j\tau) \quad (74)$$

to obtain

$$\chi_{ij}(\tau, f_D) = \sqrt{\frac{1}{\pi\lambda^2}} \exp\left(j(b_j\tau^2 + a_j\tau) - \frac{\tau^2}{2\lambda^2}\right) \times \int_{-\infty}^{\infty} \exp\left(-\alpha t^2 - \beta t\right) dt \quad (75)$$

The integral is then written in a quadratic form as

$$\chi_{ij}(\tau, f_D) = \sqrt{\frac{1}{\pi\lambda^2}} \exp\left(j(b_j\tau^2 + a_j\tau) - \frac{\tau^2}{2\lambda^2}\right) \times \int_{-\infty}^{\infty} \exp\left(-\alpha\left(t + \frac{\beta}{2\alpha}\right)^2 + \frac{\beta^2}{4\alpha}\right) dt \quad (76)$$

and finally

$$\chi_{ij}(\tau, f_D) = \sqrt{\frac{1}{\pi\lambda^2}} \exp\left(j(b_j\tau^2 + a_j\tau) - \frac{\tau^2}{2\lambda^2} + \frac{\beta^2}{4\alpha}\right) \times \int_{-\infty}^{\infty} \exp\left(-\alpha\big(t + \frac{\beta}{2\alpha}\big)^2\right) dt \quad (77)$$

The integral in (77) is of a known form that converges to $\sqrt{\pi/\alpha}$ for $\Re(\alpha) > 0$ and this condition is verified for all values of τ and f_D. This leads to the final expression of the cross-ambiguity function

$$\chi_{ij}(\tau, f_D) = \sqrt{\frac{1}{\alpha\lambda^2}} \exp\left(j(b_j\tau^2 + a_j\tau) - \frac{\tau^2}{2\lambda^2} + \frac{\beta^2}{4\alpha}\right) \quad (78)$$